A Model Macroion Solution Next to a Charged Wall: Overcharging, Charge Reversal, and Charge Inversion by Macroions

Felipe Jiménez-Ángeles and Marcelo Lozada-Cassou*

Programa de Ingeniería Molecular, Instituto Mexicano del Petróleo, Lázaro Cárdenas 152, 07730 México, D. F., México, and Departamento de Fısica, Universidad Autónoma Metropolitana-Iztapalapa, Apartado Postal 55-334, 09340 D. F. México

Received: August 19, 2003; In Final Form: February 11, 2004

We study the inhomogeneous primitive model macroion solution next to a charged wall, through an integral equations theory. We report a new class of *overcharging*, which refers to the adsorption of an effective charge onto a like-charged wall. In addition, macroions produce surface charge reversal, charge inversion, and layering. The role of electrostatic and excluded volume correlations, on these effects, is discussed. It is argued that electrostatic and the steric repulsive interactions give rise to depletion forces which produce macroion adsorption, even if the wall or the macroparticle are *uncharged* or if the wall and macroions are like charged. By consideration of two limit cases of the inhomogeneous primitive model, the role of the small ion and macroion short-range correlations is separately examined. Across the paper, the agreement is discussed of our results with computer simulations and with experimental results.

1. Introduction

The physics of macroion adsorption at charged interfaces is the subject of recent theoretical and experimental studies.[1−6] It is known that, in the neighborhood of a charged surface, low-concentrated solutions of monovalent ions produce an exponentially decaying charge distribution (known as the electrical double layer (EDL)), which is well described by the Poisson−Boltzmann (PB) equation. However, adsorption of multivalent ions displays important deviations from the PB picture.[2,5] When an electrolyte or macroion solution is next to a charged surface, oppositely charged ions (counterions) are adsorbed to the surface, forming a layer with a sign opposite to that of the surface. Under certain conditions, the charge of these counterions can overcome the surface charge. This phenomenon is known as charge reversal (CR), and as a result, the effective electrical field produced by the electrode plus counterions reverses its direction with respect to the unscreened electrode electrical field. This effective, reversed electrical field, in turn, produces a layer of like-charged ions, i.e., next to the first counterion layer. This second layer is referred to as charge inversion (CI).[7,8]

In molecular engineering, CR and CI are basic mechanisms for self-assembling polyelectrolyte layers on a charged substrate,[1] reverse mobility experiments,[9−11] self-assembled DNA−lipid membrane complexes,[12] anomalous macroion adsorption on a Lagmuir film,[2] and novel colloid stabilization mechanisms.[6] The understanding of these phenomena have been recognized as relevant for the colloid science and technology,[13,14] the oil industry, molecular self-assembly (e.g., DNA encapsulation), and nanostructured films (e.g., polyelectrolyte layering).[1,5,15]

CR was reported since the early 80s,[16,17] and some advances in its understanding have been done; however, the mechanism has not been completely understood. Some authors have recognized the relevance of electrostatic and ionic size correlations in CR.[7,8,18,19] In a recent study, Shklovskii et al.[20] considered macroions on an *oppositely* charged surface. They propose that macroions overscreening a charged surface are highly ordered in a bidimensional Wigner crystal (WC) structure, as a configuration of minimal electrostatic free energy. However, in the WC theory, ionic correlations are only considered at the level of a two-dimensional electrons liquid at *zero* temperature, which is justified only in an extremely high coupling limit,[13] and implies that short-range correlations are not considered. Nevertheless, WC theory has a good agreement with Monte Carlo simulations of a two-dimensional electron liquid[21] and zero-temperature molecular dynamics calculations of a two-dimensional layer of adsorbed ions.[22] In a study of the planar EDL for two-component 1:1 and 2:2 electrolytes, Greberg and Kjellander studied a primitive model electrolyte, considering a small size asymmetry between co-ions and counterions,[8] and presented several mechanisms to explain CR and CI.

Particle-excluded volume has the effect of reducing entropy; thus, in the literature, it is referred to as the entropy contribution. At nonzero temperature, a balance between entropy and energy is required for the occurrence of CR[19] and for other unexpected effects, as the effective attraction between like-charged particles.[23] A robust description of the EDL phenomenology must include both electrostatic interactions and the many-body hard-core interactions. Both contributions are, in principle, considered in the primitive model electrolyte; however, for very low concentration of particles and/or *zero* temperature, the effect of entropy is negligible. The simplest description of the diffuse EDL at temperature different from zero is provided by the PB theory. This approach, however, does not take into account the ion−ion hard-core interactions and, as a consequence, is inappropriate to describe the situations where these contributions are relevant.

In this work, we study a *three-component* fluid next to a charged wall. Our model macroion solution is studied through the hypernetted chain/mean spherical approximation (HNC/MSA) integral equations theory. The HNC/MSA theory is in agreement with molecular simulation data for the EDL of closely related models,[24−28] which indicates that this theory takes

* To whom correspondence may be addressed. E-mail: marcelo@imp.mx.

10.1021/jp036464b CCC: $27.50
Published on Web 05/11/2004

reasonably well into account electrostatic and excluded-volume contributions. In a recent work[29] we applied this approach to study the Donnan equilibrium, i.e., we solved the HNC/MSA equations for our model macroions solution separated from an electrolyte solution, by a semipermeable membrane. We found a good agreement with experimental data, with no use of adjustable parameters.

Here we study the adsorption mechanisms of macroions, in solution, onto a charged wall. We find a more complex kind of CR and CI, not reported before, a new phenomenon (we will refer to it as overcharging (OC)) and explain our results in term of general principles. We also analyze the particular case of an uncharged wall or uncharged colloids, the limit case of macroions in a point ions electrolyte, and a mixture of three-species point ions where, however, they interact with the wall as charged hard spheres. The two limit cases can be seen as extended versions of the PB theory.

It should be pointed out that for the two-component case we recover the results of Greberg and Kjellander. We also found a qualitative agreement with the molecular simulations of Terao and Nakayama[4] for a mixture of macroions plus counterions (with no added salt) next to a charged surface. The WC theory[20] has some similarity with our model. However, whereas we use direct (macroion−macroion, macroion−counterion, and macroion−wall) Coulombic interactions, in WC, screened interactions are used. More important, however, is the inclusion of size correlations in our theory, which are of fundamental importance for finite temperature calculations.[24]

The structure of the paper is organized as follows: In section 2, we derive in detail the HNC/MSA integral equations for the system and discuss correlations and entropy in relation with macroions adsorption. In section 3, we present results for the local concentration profiles of ions and macroions and the induced-charge profiles for three different macroions solutions models. Finally, in section 4, some conclusions are presented.

2. Theory

2.1. Integral Equations for Inhomogeneous Fluids. The method that we use to derive integral equations for inhomogeneous fluids makes use of a simple fact: In a fluid, an external field can be considered simply as another particle in the fluid, i.e., as an additional infinitely dilute species in the fluid. This statement is valid in general. However, it is particularly useful in the statistical mechanics theory for inhomogeneous fluids, as it has been shown in the past.[30,31] Below, we apply this method to a model inhomogeneous macroion solution.

The multicomponent Ornstein−Zernike (OZ) equation for an homogeneous fluid made up of $n + 1$ species is

$$h_{ij}(\mathbf{r}_{21}) = c_{ij}(\mathbf{r}_{21}) + \sum_{m=1}^{n+1} \rho_m \int h_{im}(\mathbf{r}_{23}) c_{mj}(\mathbf{r}_{13})\, \mathrm{d}v_3 \quad (1)$$

where ρ_m is the concentration of species m, $h_{ij}(\mathbf{r}_{21}) \equiv g_{ij}(\mathbf{r}_{21}) - 1$ and $c_{ij}(\mathbf{r}_{21})$ are the total and direct correlation functions for two particles at $\mathbf{r}_2$ and $\mathbf{r}_1$ of species i and j, respectively, $g_{ij}(\mathbf{r}_{21})$ is the pair distribution, and $\mathbf{r}_{21} = \mathbf{r}_2 - \mathbf{r}_1$. To solve eq 1, we need an additional relationship between the $h_{ij}(\mathbf{r}_{21})$ and $c_{ij}(\mathbf{r}_{21})$ functions, known as closures. The derivation of a particular functional relation between these two functions (closures) is the subject of the many-body theory of liquids, and different theories really define different types of quasiparticles. The formal derivation of these closures is based on diagrammatic expansions, which are grouped according to their topological properties and later counted with sophisticated combinatorial techniques.[31−33] Among the most known closures between $h_{ij}(\mathbf{r}_{21})$ and $c_{ij}(\mathbf{r}_{21})$ are

$$c_{ij}(\mathbf{r}_{21}) = -\beta u_{ij}(\mathbf{r}_{21}) + h_{ij}(\mathbf{r}_{21}) - \ln g_{ij}(\mathbf{r}_{21}) \quad (2)$$

$$c_{ij}(\mathbf{r}_{21}) = -\beta u_{ij}(\mathbf{r}_{21}) \quad (3)$$

Equations 2 and 3 are known as the hypernetted chain (HNC) and the mean spherical (MSA) approximations, respectively; $u_{ij}(\mathbf{r}_{21})$ is the direct interaction potential between two particles of species i and j, and $\beta \equiv 1/k_B T$. Some more possibilities to solve eq 1 are originated by considering a closure for $c_{ij}(\mathbf{r}_{21})$ in the first term of eq 1 and a different one for $c_{mj}(\mathbf{r}_{13})$ in the second term of eq 1, giving rise to hybrid closures.

We let an external field be one of the fluid species, say $(n + 1)$ species (denoted as the γ species), which is required to be infinitely dilute, i.e., $\rho_\gamma \to 0$. Therefore, from eq 1, the total correlation function between a γ species particle and a j species particle is given by

$$h_{\gamma j}(\mathbf{r}_{21}) = c_{\gamma j}(\mathbf{r}_{21}) + \sum_{m=1}^{n} \rho_m \int h_{\gamma m}(\mathbf{r}_{23}) c_{mj}(\mathbf{r}_{13})\, \mathrm{d}v_3 \quad \text{with} \quad j = 1, ..., n \quad (4)$$

The total correlation functions for the remaining species, i.e., the fluid species, satisfy a n-component OZ equation, eq 1 (with no γ species), from which $c_{mj}(\mathbf{r}_{13})$ is obtained.

In this scheme, the pair correlation functions, $g_{\gamma j}(\mathbf{r}_{21}) \equiv h_{\gamma j}(\mathbf{r}_{21}) + 1$, is the inhomogeneous one-particle distribution function, $g_j(\mathbf{r})$, for particles of species j under the influence of an external field (produced by a particle of species γ). The local concentration profile for the j species is given by $\rho_j(\mathbf{r}) = \rho_j g_j(\mathbf{r})$, where $g_j(\mathbf{r})$ is the reduced concentration profile (RCP).

In this work, we will use a hybrid closure, in which the HNC (eq 2) closure is used for the $c_{\gamma j}(\mathbf{r}_{21})$ and the MSA closure (eq 3) for $c_{mj}(\mathbf{r}_{13})$. Therefore, eq 4 becomes

$$g_{\gamma j}(\mathbf{r}_{21}) = \exp\{-\beta u_{\gamma j}(\mathbf{r}_{21}) + \sum_{m=1}^{n} \rho_m \int h_{\gamma m}(\mathbf{r}_{23}) c_{mj}(\mathbf{r}_{13})\, \mathrm{d}v_3\} \quad (5)$$

As we pointed out above, $c_{mj}(\mathbf{r}_{13})$ is approximated by the direct correlation function for a n-component homogeneous fluid. Hence, by use of the $c_{mj}(\mathbf{r}_{13})$ function obtained from MSA in eq 5, we obtain the HNC/MSA equation for an inhomogeneous fluid. This equation has shown to be particularly successful in the case of inhomogeneous charged fluids when it is compared with molecular simulation data.[24−28]

2.2. The Model. A simple model for a n-component electrolyte is that where the ions are considered to be hard spheres, bearing a centered point charge. This model is known as the primitive model electrolyte and includes the two relevant forces of the system: the (long-range) electrostatic and the (short-range) hard-core interactions. The two-component case of this model, in which particles are considered size symmetric, is called the restricted primitive model (RPM) electrolyte solution.

In this paper, we model our system through an *inhomogeneous* primitive model (IPM): We consider a uniformly charged planar hard wall, with σ_0 charges per unit area, next to a fluid phase which contains macroions plus a two-component electrolyte. The fluid is modeled through the primitive model electrolyte; hence, the fluid components are considered to be

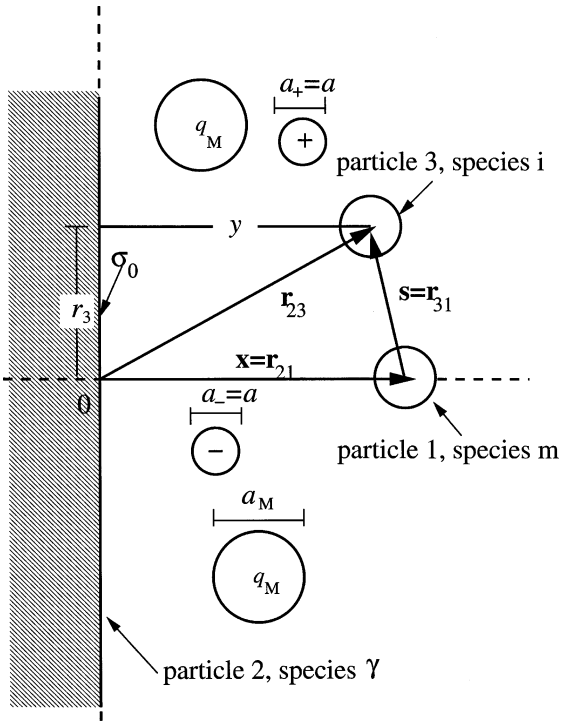

Figure 1. Schematic representation of the inhomogeneous primitive model.

charged hard spheres, with charge $q_i = z_i e$ (where e is the protons's charge and z_i is the valence number), diameter a_i, and concentration ρ_i, with $i = 1, \ldots, 3$. We label cations as species 1, the anions as species 2, and the macroions as species 3. Therefore, we use the following notation, $\rho_+ \equiv \rho_1$, $\rho_- \equiv \rho_2$, and $\rho_M \equiv \rho_3$, for the anions, cations, and macroions concentrations, respectively, idem for a_i and z_i. Besides, the fluid is subject to the bulk electroneutrality condition, i.e.,

$$\sum_{i=1}^{3} z_i \rho_i = 0 \tag{6}$$

A schematic representation of the model is found in Figure 1. Two ions of species i and j, with relative position r, interact via the following potential

$$u_{ij}(r) = \begin{cases} \infty & \text{if } r < a_{ij} \\ \dfrac{z_i z_j e^2}{\epsilon r} & \text{if } r \geq a_{ij} \end{cases} \tag{7}$$

with $i, j = 1, \ldots, 3$ and $a_{ij} \equiv (a_i + a_j)/2$. The mixture is embedded in a continuous media of dielectric constant ϵ, set equal to that of the charged surface in order to avoid image charges. The charge on the surface is compensated by an excess of charge in the fluid; hence, it is satisfied

$$-\sigma_0 = \int_0^\infty \rho_{el}(x)\, dx \tag{8}$$

where $\rho_{el}(x) = \sum_{i=1}^{3} q_i \rho_i(x)$ and $\rho_i(x)$ is the local concentration profile of the ith species. According to the integral equations method outlined in section 2.1, the surface is considered as the fluid species labeled as γ (see Figure 1). The interaction between the surface and an i-species particle, $u_{\gamma i}(r_{21})$, is split as $u_{\gamma i}(x) = u_{\gamma i}^{el}(x) + u_{\gamma i}^{*}(x)$, where $u_{\gamma i}^{el}(x)$ is the direct electrostatic potential and $u_{\gamma i}^{*}(x)$ is the hard-core interaction. The former can be found from Gauss' law, resulting in

$$-\beta u_{\gamma i}^{el}(x) = \left\{ \frac{2\pi}{\epsilon} z_i e \beta \sigma_0 (x - L) \quad \text{for} \quad x \geq 0 \right. \tag{9}$$

where x is the particle position referred to a coordinates system set at the surface and measured perpendicularly and L is the location of a reference point.

The hard-core interaction is given by

$$u_{\gamma i}^{*}(x) = \begin{cases} \infty & \text{if } x < \dfrac{a_i}{2} \\ 0 & \text{if } x \geq \dfrac{a_i}{2} \end{cases} \tag{10}$$

for $i = 1, \ldots, 3$.

In this geometry, $g_{\gamma i}(\mathbf{r}_{21})$ depends only on the perpendicular position to the plate, i.e., $g_{\gamma i}(\mathbf{r}_{21}) = g_{\gamma i}(x)$; hence, we will use $\mathbf{r}_{21} = \mathbf{x}$ and $\mathbf{r}_{31} = \mathbf{s}$ (see Figure 1).

By use of MSA, the $c_{mj}(\mathbf{r}_{13})$ function for a primitive model electrolyte has an analytical expression written as

$$c_{mj}(s) = -\beta u_{mj}^{el}(s) + c_{mj}^{sr}(s) + c_{mj}^{hs}(s) \tag{11}$$

where $s \equiv |\mathbf{r}_{13}|$ is the relative distance between two ions of species m and j. In the first term appears the direct electric interaction potential between two ions, given by the second term of eq 7, $c_{mj}^{sr}(s)$ and $c_{mj}^{hs}(s)$ are functions (given explicitly in appendix A) responsible for the particle's *short-range* correlations. Taking advantage of the cylindrical geometry, we use $d\upsilon_3 = 2\pi r_3\, dr_3\, dy$ and $s^2 = x^2 + r_3^2 + y^2 - 2xy$; after some algebra, eq 5 is written as[34,35]

$$g_{\gamma i}(x) = \exp\{-\beta z_i e \psi(x) + 2\pi \sum_{j=1}^{3} \rho_j \int_{a_j/2}^{\infty} h_{\gamma j}(y)[K_{ji}(x,y) + L_{ji}(x,y)]\, dy - 2\pi A_i(x)\} \tag{12}$$

or equivalently

$$g_{\gamma i}(x) = \exp\{-\beta z_i e \psi(x) - \beta J_{\gamma i}(x)\} \tag{13}$$

where $J_{\gamma i}(x)$ is given by

$$J_{\gamma i}(x) = -2\pi k_B T \sum_{j=1}^{3} \rho_j \int_{a_j/2}^{\infty} h_{\gamma j}(y)[K_{ji}(x,y) + L_{ji}(x,y)]\, dy + 2\pi k_B T A_i(x)$$

and with the mean electrostatic potential, $\psi(x)$, given by

$$-\beta z_i e \psi(x) = \frac{4\pi}{\epsilon} z_i e \beta \sigma_0 x + 2\pi z_i \frac{e^2 \beta}{\epsilon} \sum_{j=1}^{3} z_j \rho_j \int_{a_j/2}^{\infty} g_{\gamma j}(y)[x + y + |x - y|]\, dy \tag{14}$$

The term $J_{\gamma i}(x)$ contains the contribution of short-range correlations to the ion surface potential of mean force. According to eq 12, both $\psi(x)$ and $J_{\gamma i}(x)$ are functionals of $\rho_i(x)$; thus, in this theory, charge and size correlations are in general *not independent*.

The mean electrostatic potential, $\psi(x)$, satisfies Poisson's equation

$$\nabla^2\psi(x) = -\frac{4\pi}{\epsilon}\rho_{el}(x) \quad \text{with} \quad \rho_{el}(x) = \sum_{i=1}^{3} z_i e \rho_i g_{\gamma i}(x) \quad (15)$$

The expressions for the kernels, $K_{ji}(r,y)$ and $L_{ji}(x,y)$, are given in appendix A.

We will discuss our model in terms of the reduced concentration profiles of the three species, $g_{\gamma i}(x)$, and the local net charge per unit area, $\sigma(x)$, where

$$\sigma(x) = \sigma_0 + \sigma'(x) \quad \text{with} \quad \sigma'(x) \equiv \int_0^x \rho_{el}(y)\, dy \quad (16)$$

As pointed out above, σ_0 is the surface charge density and $\sigma'(x)$ is the induced charge in the fluid, from zero to the distance x to the plate. The electroneutrality condition, eq 8, implies $\lim_{x\to\infty}\sigma'(x) \to -\sigma_0$ to have thermodynamical equilibrium. In the PB description of a simple electrolyte, if $\sigma_0 > 0$, $\sigma(x)$ monotonically decreases from $\sigma(a/2) = \sigma_0$ to $\sigma(x) = 0$ as $x \to \infty$. However, in general, $\sigma(x)$ will oscillate around zero, i.e., if $\sigma_0 > 0$, $\sigma(x)$ can be larger than σ_0 (overcharging), negative (charge reversal), or positive (charge inversion).

The reduced concentration profiles ($g_{\gamma i}(x)$) are defined in terms of the ion-surface potential of mean force, $w_{\gamma i}(x)$, by

$$g_{\gamma i}(x) \equiv \exp\{-\beta w_{\gamma i}(x)\} \quad (17)$$

thus, from eq 13

$$w_{\gamma i}(x) = -k_B T \ln(g_{\gamma i}(x)) = z_i e \psi(x) + J_{\gamma i}(x) \quad (18)$$

The effective electrostatic force on an ion of species i is

$$f_i^e(x) \equiv -e z_i \frac{\partial\psi(x)}{\partial x} = \frac{4\pi e z_i}{\epsilon}\sigma(x) \quad (19)$$

Therefore, $\sigma(x)$ is not only a measure of CR and CI but also of the wall particle effective electrical force. From eqs 17 and 18, the effective net force between the wall and an ion of species i is written as

$$F_i(x) = -\frac{\partial w_{\gamma i}(x)}{\partial x} = \frac{1}{\beta}\frac{\partial \ln(g_{\gamma i}(x))}{\partial x} = f_i^e(x) + f_i^s(x) \quad (20)$$

where $f_i^s(x) \equiv -\partial J_{\gamma i}(x)/\partial x$ contains the nonelectrostatic contributions, i.e., the ionic excluded-volume contributions. However, it should be pointed out that, although $f_i^e(x)$ and $f_i^s(x)$ can be identified as two different forces, they are really interconnected through eq 12.

2.3. Correlations and Entropy. The magnitude and direction of $F_i(x)$ is ruled by several effects, which, in turn, dictate the adsorption (desorption) of particles to the charged wall. The role of the surface−particle direct electrostatic interaction is well understood: the lower the electrostatic energy at the surface

$$\left[U_{\gamma i} = q_i u_{\gamma i}\left(\frac{a_i}{2}\right) = \frac{2\pi}{\epsilon} q_i \sigma_0\left(L - \frac{a_i}{2}\right)\right]$$

particles adsorption is energetically more favorable. From this simple formula, it is clear that particles with a higher valence or a higher opposite surface charge density increase particle adsorption. In our study, we will focus on the many-body correlations, which are responsible for the surface−particle forces of electrostatic and nonelectrostatic origin. The discussion of the phenomena reported here is carried out in terms of the hard-core and Coulomb coupling correlations. The particles volume fraction given by

$$\eta_T \equiv \frac{\pi}{6}\sum_i \rho_i a_i^3 \quad (21)$$

accounts for the steric contribution, whereas the strength of the Coulombic interaction is quantified by means of the parameter ξ_{ij}, given by

$$\xi_{ij} \equiv \frac{\beta}{\epsilon}\frac{q_i q_j}{a_{ij}} \quad (22)$$

Therefore, the effects produced by varying z_i, ρ_i, a_i, etc., will be discussed in terms of the ξ_{ij} and η_T parameters, i.e., in terms of the excluded-volume and electrostatic correlations.

Thermodynamically, the effect of correlations is reflected on the system entropy: From basic statistical mechanics, the canonical equilibrium entropy for an *homogeneous bulk* fluid, constituted by N interacting particles in a volume V, is given by

$$S^{bulk} \equiv S^{id} + k_B\left[\frac{\partial T \ln(Z_N/V^N)}{\partial T}\right]_{N,V} \quad (23)$$

where $S^{id} = 5/2Nk_B - Nk_B \ln(\Lambda^3\rho)$, where $\Lambda = (\beta h^2/2\pi m)^{1/2}$, the deBroglie thermal length, and

$$Z_N = \int ... \int \exp\{-\beta U_N\}\, d\mathbf{r}_1, ..., d\mathbf{r}_N \quad (24)$$

being the partition function and U_N the potential energy of the N interacting particles. A simple analysis of the expression for S^{id} indicates that (for constant N) it is lower as ρ augments, i.e., as V decreases. For a fluid made up of N interacting *hard spheres*, of diameter a, the value of Z_N and S^{bulk} follow the tendency dictated by the *accessible volume fraction*, υ^*, i.e., if υ^* decreases (increases), the value of Z_N and S^{bulk} decreases (increases). On the other hand, υ^* is related to the particle's excluded volume, υ, by $\upsilon^* = (V - \upsilon)/V$.[36] We assume that a reasonable estimation for υ, for a hard spheres fluid, is provided by the expression for the excluded volume of N hard spheres in a face-centered cubic crystal, which is given by $\upsilon = \pi/6Na^3$, and thus, $\upsilon^* \approx 1 - \pi/6\rho a^3$.

In the presence of a planar hard wall, a hard-spheres fluid is an inhomogeneous fluid with an entropy S^{inh}. By adsorbing particles to the wall, the system increases the accessible volume (υ^*) and, thus, the system gains entropy[37,38] with respect to the bulk conditions, i.e., $S^{inh} > S^{bulk}$. From a mechanistic point of view, the adsorption of hard spheres is due to an effective force on particles toward the wall. In terms of eq 20, $F_i(x) = f_i^s(x) < 0$, which is conceived as of entropic origin. In hard-spheres fluids, the magnitude of depletion attractive forces, and hence the adsorption, enhances as the particle's excluded volume increases, i.e., as $\eta = \pi/6\rho a^3$ increases.

For the present study, we consider a model macroion next to a planar hard wall, which was considered to be *charged* or *uncharged*. Therefore, not only the steric contribution dictates the tendencies of S^{bulk}, S^{inh}, and the particle's adsorption, but in addition, they are modified by the presence of the electrostatic correlations. On the function S^{bulk}, particle−particle repulsive interactions (which is the case for the macroion−macroion electrostatic interaction) produce a similar effect as in the pure hard-core interaction, i.e., the more repulsive the interaction,

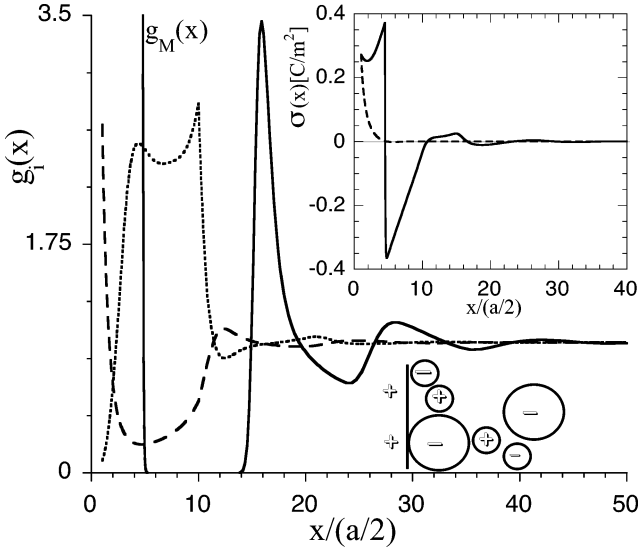

Figure 2. Inhomogeneous RCPs, as a function of x, for macroions (solid line), anions (dashed line), and cations (dotted line) next to a positively charged wall ($\sigma_0 = 0.272$ C/m^2). The fluid contains macroions ($z_M = -40$, $\rho_M = 0.01$ M, $a_M = 4.5a$) in a 2:1 electrolyte solution ($\rho_+ = 0.7$ M, $\rho_- = 1.0$ M, $z_+ = 2$, $z_- = -1$). In the inset, the solid line is the charge density profile, $\sigma(x)$, as a function of x, for the macroion solution, whereas the dashed line is $\sigma(x)$ for a 2:1 RPM electrolyte ($\rho_+ = 0.5$ M, $\rho_- = 1.0$ M, $z_+ = 2$, $z_- = -1$), with *no* macroions. The sketch roughly represents the distribution of ions indicated by their RCP. These profiles were obtained from the HNC/MSA theory applied to the IPM.

the higher the fluid excluded volume and hence the lower the value of S^{bulk}. *Thus, in an inhomogeneous fluid, the repulsive interactions are expected to increase the tendency of particles to be adsorbed to the wall, in analogy with the pure hard spheres fluid. Therefore, one can expect that higher values of η_T and ξ_{ii} produce a more negative value of $F_i(a_i/2)$ and, hence, increase the adsorption of particles to the surface. These two parameters, together with $U_{\gamma i}$, are expected to rule the mechanisms of particles adsorption.*

3. Results for the IPM

We solve HNC/MSA (eq 12) using a sophisticated finite-element technique.[39] Typically, the time needed for the solution with a given set of parameters is less than 10 min. We present results for several values of z_M, a_M, ρ_M, σ_0, and salt parameters z_+, z_-, ρ_i, and a. In all our calculations, we have used fixed values of $a = a_+ = a_- = 4.25$ Å, $T = 298$ K, and $\epsilon = 78.5$. In the rest of the paper, we omitted the γ subindex for simplicity.

In Figure 2, the macroion has a negative charge ($z_M = -40$, $\rho_M = 0.01$ M), which is opposite to that of the wall ($\sigma_0 = 0.272$ C/m^2) and is in an electrolyte solution ($z_+ = 2$, $z_- = -1$, $\rho_+ = 0.7$ M, and $\rho_- = 1$ M). The macroion reduced concentration profile (RCP) shows a very strong adsorption to the wall. The RCP, for the positive small ions, show that macroions of the first layer are surrounded by their counterions; therefore, macroions come accompanied to the positive wall surrounded by divalent cations. At the wall's neighborhood, cations outnumber anions, and this in turn appears as an effective positive charge next to the wall. *Such an effect defines a new phenomenon, hereinafter referred to as overcharging (OC), i.e., at the wall's neighborhood we find the accumulation of an effective additional charge with the same sign of the wall. This effect is due to the strong electrostatic attraction between macroions and the divalent cations. However, for this effect to be present, a high particle's excluded volume is needed, i.e., a high concentration of macroions and/or little particles and/or large macroion size or little ion size.* Although it is not shown, we have corroborated this statement by numerous calculations. To the best of our knowledge, this effect has not been reported before. If the particle's excluded volume is not high enough, i.e., low η_T, OC does not occur. For the high value of $\sigma_0 = 0.272$ C/m^2, to see OC, it is necessary to have a high Coulombic coupling between cations and macroions, ξ_{M+}. However, OC occurs even if ξ_{M+} and σ_0 are not very high but η_T is high.

A second layer of macroions is adsorbed, with an intermediate layer of divalent positive ions, followed by monovalent negative little ions. A layer of positive divalent ions, followed by a monovalent negative ions layer, also mediates a third layer of adsorbed negative macroions. Subsequent layers of less concentrated macroions are observed, which are also mediated by layers of positive and negative little ions. Therefore, for these conditions, we observe not only a surface CR produced by macroions but also macroions multilayering. Considering that the bulk macroion concentration is 0.01 M, the local macroion concentration at the second peak, ~0.035 M, is not negligible. The local macroion concentration in contact with the wall is $\rho_M(a_M/2) \equiv \rho_M g_M(a_M/2) \approx 21$ M. Hence, large macroions next to a highly charged wall *assemble* next to the wall. In the inset, at a distance of one macroion radius ($x = a_M/2$), a deep minimum is observed, corresponding to a very strong CR produced by the first layer of macroions. The maximum located around $15a/2$ shows a CI. For x lower than one macroion radius, i.e., $x \leq a_M/2$, OC is present: That is, the wall's divalent coions are accumulated next to the wall and their charge exceeds that of the wall plus the adsorbed negative little ions. This effect is probably present only in macroion solutions. The word *overcharging* deserves a little comment: In the literature, OC has been indistinctly used in reference to charge reversal and charge inversion. However, the word overcharging implies an excess of charge. Thus the new phenomenon, here referred to as OC, should not be confused with CR or CI.

The effective wall electrical field, which is proportional to $\sigma(x)$, is positive before the first layer of macroions and then negative, before the second layer (see inset in Figure 2). Hence, the electrical force is first attractive and then repulsive to negative ions. The behavior of the total force on an ion of species i, however, is implicit in the RCP, i.e., a derivative of $g_i(x)$ above (below) 0 implies that $F_i(x)$ is repulsive (attractive). At $x = a/2$, $\sigma(x)$ is equal to the wall's charge, whereas for $x \rightarrow \infty$, $\sigma(x) \rightarrow 0$, as it should be if electroneutrality is satisfied. Lower wall charge density or lower macroion charge, size, or concentration produce lower adsorption. The 2:1 electrolyte solution (with no macroions), where the monovalent ions are the wall counterions, does not show CR nor OC (see inset in Figure 2). Hence, for monovalent little ions, there is not charge reversal. This is also the case for the $\sigma_{PB}(x)$ obtained via eq 26, i.e., the PB equation for a point ion model for pure electrolytes (not shown). In fact, the classical PB theory does not predict CR or CI for any ionic valence or concentration, and $\sigma_{PB}(x)$ is always a monotonic function and $|\sigma_{PB}(x)| \leq |\sigma_0| \; \forall \; x \in [0,\infty)$. An important difference between the PB description and the HNC/MSA theory is that, in the former, ionic size is completely neglected. However, as we will discuss below, this is not always the case if a mixture of point ions and macroions are considered. *An increment of ion size, concentration, charge, and/or wall charge implies larger values of ξ_{ij}, η_T, and $-U_{\gamma i}$ and will produce a larger macroion adsorption next to the wall and will enhance the macroion layering. Also OC, CR, and CI will be enhanced.*

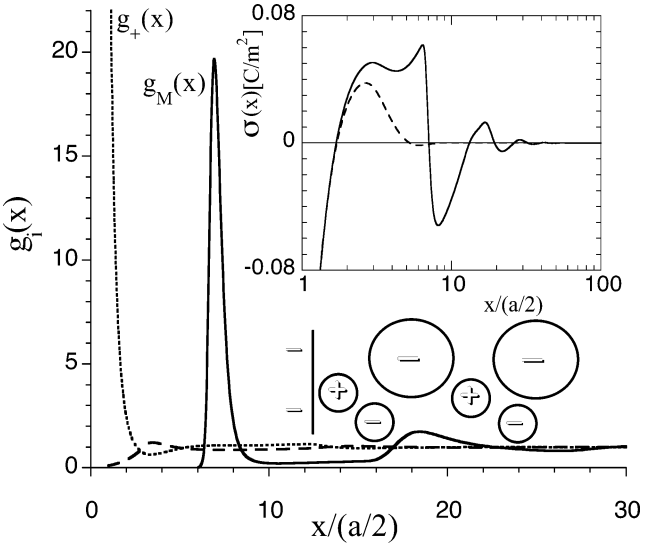

Figure 3. Inhomogeneous RCPs, as a function of x, for macroions, anions, and cations next to a negatively charged wall ($\sigma_0 = -0.272$ C/m^2). In the inset, $\sigma(x)$ is plotted for the IPM and for an inhomogeneous 2:1 RPM electrolyte ($\rho_+ = 0.5$ M, $\rho_- = 1.0$ M, $z_+ = 2$, $z_- = -1$). The lines and the fluid parameters are as in Figure 2. The sketch roughly represents the distribution of ions indicated by their RCP. These profiles were obtained from the HNC/MSA theory applied to the IPM.

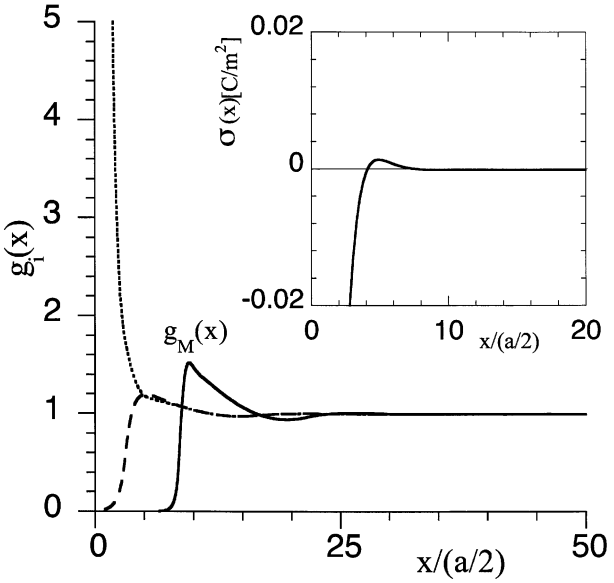

Figure 4. Inhomogeneous RCPs, as a function of x, for a mixture of *uncharged* colloids ($z_M = 0$, $a_M = 6.5a$) in a 1:1 electrolyte ($z_+ = -z_- = 1$, $\rho_+ = \rho_- = 1.0$ M) next to a negatively charged wall ($\sigma_0 = -0.272$ C/m^2). In the inset, $\sigma(x)$ is plotted for the mixture. The lines are as in Figure 2. These profiles were obtained from the HNC/MSA theory applied to the IPM.

In Figure 3, the fluid parameters are the same as in Figure 2 ($z_M = -40$, $\rho_M = 0.01$ M, $z_+ = 2$, $z_- = -1$, $\rho_+ = 0.7$ M, and $\rho_- = 1$ M), but the wall has a negative charge ($\sigma_0 = -0.272$ C/m^2), i.e., the macroions and the wall are like charged. Here, the positive divalent little ions are counterions of the wall and macroion. A layer of positive ions followed by negative ions is adsorbed to the wall, which produces a strong surface charge reversal and mediates a strong adsorption of macroions. The first peak corresponds to a 0.2 M macroion concentration, which implies a CI produced by macroions. In the inset, a CR is followed by a CI. In Figure 2, the macroions are responsible for the first CR, whereas in Figure 3, they are responsible for the first CI. In Figure 3, in the absence of macroions, the 2:1 electrolyte does show CR. Thus, if no macroions are present, *little* monovalent counterions do not produce CR, whereas divalent counterions do (compare the insets in Figures 2 and 3). Clearly CR observed in the inset of Figure 3, for the pure electrolyte solution, is due to the divalent nature of counterions. Hence, CR in this case is obtained as a result of the attractive electrostatic energy between the wall and the divalent ions. This energy, $U_{\gamma i}$, is not enough to produce CR when counterions are monovalent. However, electrostatic energy is not all one has to consider since for divalent point counterions CR is not observed. Hence, ionic excluded volume must play a role since this is the main difference between the RPM and the point ions model used in the PB theory. Indeed, in the past,[24] we have shown through integral equations and MD calculations that the RPM does not show CR for sufficiently small *divalent* counterions, and it does show CR for sufficiently large *monovalent* counterions. These results are consistent with our previous analysis in terms of ξ_{ij}, η_T, and $U_{\gamma i}$. *Even though the wall and macroions are like charged, and hence,* $U_{\gamma M} > 0$, *because* ξ_{Mi} *and* η_T *are large we have macroions adsorption, although mediated by a layer of little positive ions.*

These findings are consistent with recent MD results where large monovalent counterions are shown to produce CR.[17,24] They are also consistent with Figure 9 of ref 3 by Tanaka and Grosberg and Figure 4 of ref 40 by Terao and Nakayama, where CR is seen to increase with particles concentration.

In Figure 4, *uncharged* large particles, immersed in a 1:1 RPM electrolyte are next to a negatively charged wall. A slight CR is observed in the inset, even though the counterions are monovalent. EDL studies for pure 1:1 electrolytes show that there are not induced charge density or RCP oscillations.[25] Hence, in Figure 4, the oscillations in the little ions RCP are due to size correlations related to the macroparticle adsorption to the wall. *Thus, macroion charge is not necessary to have macroparticle adsorption, and their presence induces ionic oscillations for 1:1 electrolytes. In this case, the surface CR is caused by the strong depletion forces on the ions, which are due to the high colloids excluded volume. Hence it is the fact that* η_T *has increased due to the presence of the uncharged particles that we see CR.*

In Figure 5 the wall is *uncharged*. The result is an important adsorption of macroions to the wall. The local macroion concentration, at contact with the wall is $\rho_M(a_M/2) \approx 3.2$ M. The ion and macroion profiles imply an induced-charge distribution in the fluid ($\rho_{el}(x)$), which satisfies $\int_0^\infty \rho_{el}(x)\, dx = 0$ because of the absence of charge on the wall. We observed that the contact value of the macroions RCP, $g_M(x = a_M/2)$, grows when particles excluded volume increases. This tendency is expected from the knowledge of systems of pure hard spheres next to walls in which adsorption increases by increasing the particles volume fraction, η_T, so that a qualitatively similar behavior is observed if a_M is increased and ρ_M is kept constant. We compared these results for the charged colloid with those for an uncharged colloid solution (not shown). The discrepancies between the RCPs for charged and uncharged colloids (at the same concentration) can be attributed to the colloid−colloid electrostatic correlations, which are absent in the case of the uncharged colloid solutions. Therefore, we see that electrostatic many-body correlations contribute with a sort of depletion force toward the wall. *In other words, the macroion−macroion electrostatic repulsion,* ξ_{MM}*, acts in a similar way as the hard-core interactions,* η_T*, such that a higher macroions charge gives the appearance of a higher macroion excluded volume and produces a higher macroion adsorption.* In the inset, strong positive and negative OC of the wall is seen. Notice the

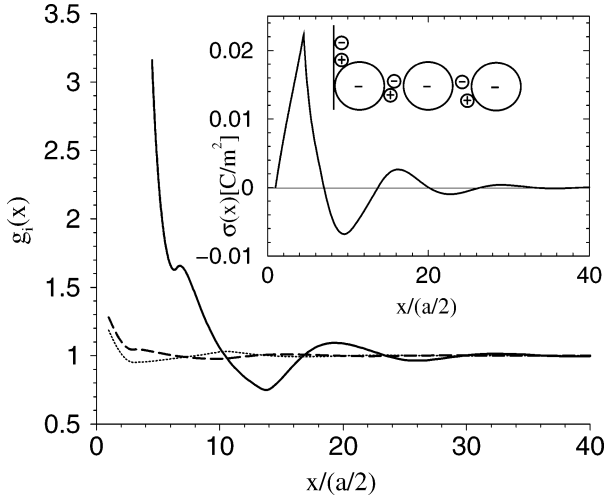

Figure 5. Inhomogeneous RCPs, as a function of x, for macroions, anions, and cations next to an *uncharged* wall ($\sigma_0 = 0$). In the inset, $\sigma(x)$ is plotted. The lines and the fluid parameters are as in Figure 2. The sketch roughly represents the distribution of ions indicated by their RCP. These profiles were obtained from the HNC/MSA theory applied to the IPM.

accumulation of an effective positive charge for $x \in [a/2, a_M/2]$. If no macroions are present, $\sigma(x) = 0$, $\forall\ x > 0$. Since the wall is uncharged, the strong macroion adsorption and wall OC is due to the ion−macroion electrostatic correlations, ξ_{MM}, ξ_{Mi}, and ξ_{ii}, and to the large excluded volume, imposed by the macroion size. It is important to point out that the OC decreases and can be undetectable if the particle's excluded volume is not high enough, even for a strong ion−macroion Coulomb coupling. These results are consistent with experiments where the *formation of nanoparticle halos around neutral microparticles* have been found to be as an important stabilization mechanism for colloids.[6]

The zero temperature WC theory[20] cannot properly describe CR. According to WC, higher salt concentration reduces CR and predict that there is a minimum charge of wall or macroion for the occurrence of CR. Contrary to WC, our results show that, depending on the macroion size, there is not a minimum wall or macroion charge for the occurrence of OC and that increasing excluded volume increases CR.[3,24,40] A semiphenomenological theory presented by Levin[13] also predicts, correctly, that higher salt concentrations increase CR. *The fact that less accessible volume imposes more order at the interface, a decrease of* S^{bulk}, *an increase of* S^{inh}, *and more adsorption to the wall, as discussed above, is consistent with the results presented here.* The higher adsorption of macroions as the accessible volume fraction, $v^* = 1 - \eta_T$, decreases can be seen from the general expression for entropy (eq 23), in terms of the partition function. Clearly, from eq 24, the larger the little ion or macroion size or their concentration, the lower Z_N and, hence, the configurational entropy. The lower the bulk entropy, S^{bulk}, the higher the molecular ordering at the wall. This statement has been validated by comparing a set of systems in equilibrium (with different particles volume fraction) and should not be confused with the increase of the inhomogeneous system entropy S^{inh}, as discussed above.

3.1. Simpler Models. A main point of our paper is the role of the short-range correlations or, better, the role of excluded volume and entropy in the adsorption mechanisms. The equations derived in section 2.2 are for a model in which both electrostatic and short-range correlations are considered. To better evaluate the role of short-range correlations, additionally, we will consider two limit cases of the IPM.

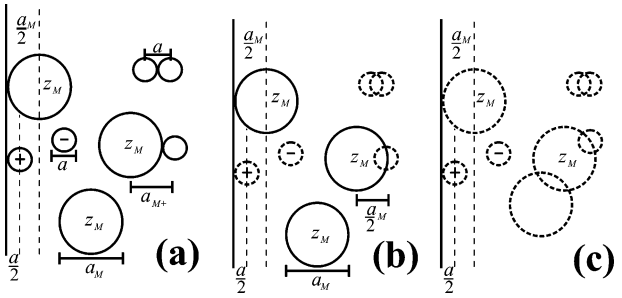

Figure 6. Different models for a macroion solution next to a charged wall. The small and large circles drawn with continuous lines represent hard charged particles of diameter a and a_M, respectively. The dotted circles represent point charges. The dashed vertical lines represent the closest approach of particles to the wall: (a) IPM; (b) IEPIM; (c) PIM.

A possible limit case of the IPM is that in which we consider little anions and cations as point charges, i.e., with $a = 0$. Therefore, the closest approach distance, $a_{ij} = a_{ji}$, between two particles of species i and j is

$$a_{ij} = \begin{cases} 0 & \text{if } i, j = +, - \\ a_M/2 & \text{if } i = M \text{ and } j = +, - \\ a_M & \text{if } i, j = M \end{cases} \qquad (25)$$

where $a_M \neq 0$ is the macroion diameter. Hence, in this simpler model the little ions interact as point charges, while we keep the macroion size. An additional desirable consideration for this model is the inclusion of a distance of closest approach of the little ions to the wall, i.e., the small ions can come close to the wall to a minimum distance $a_i/2 \equiv a/2 \neq 0$ for $i = +, -$. In other words, the little ions do have a diameter, a_i, when interacting with the wall. Such a consideration is known as the Stern correction. We will refer to this model as the inhomogeneous extended point ion model (IEPIM). So, this model is that of a macroion species in a point ion electrolyte (See Figure 6b).

An even simpler model is that in which both macroions and little ions are point ions, i.e., $a_i = 0$ for $i = +, -, M$; therefore, $a_{ij} = 0$ for $i, j = +, -, M$. We also consider the Stern correction for the three ionic species, i.e., the closest approach distances of particles to the wall are $a_i/2$ for $i = +, -, M$. In eq 12, if we neglect short-range correlations (i.e., $J_{\gamma i}(x) = 0$) and with eq 15, we get

$$\nabla^2\psi(x) = -\frac{4\pi}{\epsilon}\sum_{i=1}^{3} z_i e \rho_i \exp\{-\beta z_i e \psi(x)\} \qquad (26)$$

which is the PB equation for the EDL, i.e., HNC/MSA → PB as $J_{\gamma i} \to 0$. The values of a_i are used as boundary conditions for the integrals of $g_{\gamma i}(x)$ (see eq 14). We will refer to this model as the point ion model (PIM).

Figure 6 serves to schematically illustrate the differences among the three models, i.e., among the (a) IPM, (b) IEPIM, and (c) PIM.

To study these models, we will solve eq 12 modified to consider just the macroions diameter, in the case of the IEPIM, or no ionic size for all the ionic species, in the case of the PIM. In the following results, for all cases $a_M = 4.5a$, $a = 4.25$ Å, $z_M = -40$, $z_+ = 2$, $z_- = -1$, $\rho_M = 0.01$ M, $\rho_+ = 0.7$ M, $\rho_- = 1.0$ M, $T = 298$ K, and $\epsilon = 78.5$. These parameters are the same as those used in Figures 2, 3, and 5.

In Figure 7, we present the RCPs for macroions, anions, and cations, next to a positively charged wall ($\sigma_0 = 0.272$ C/m^2)

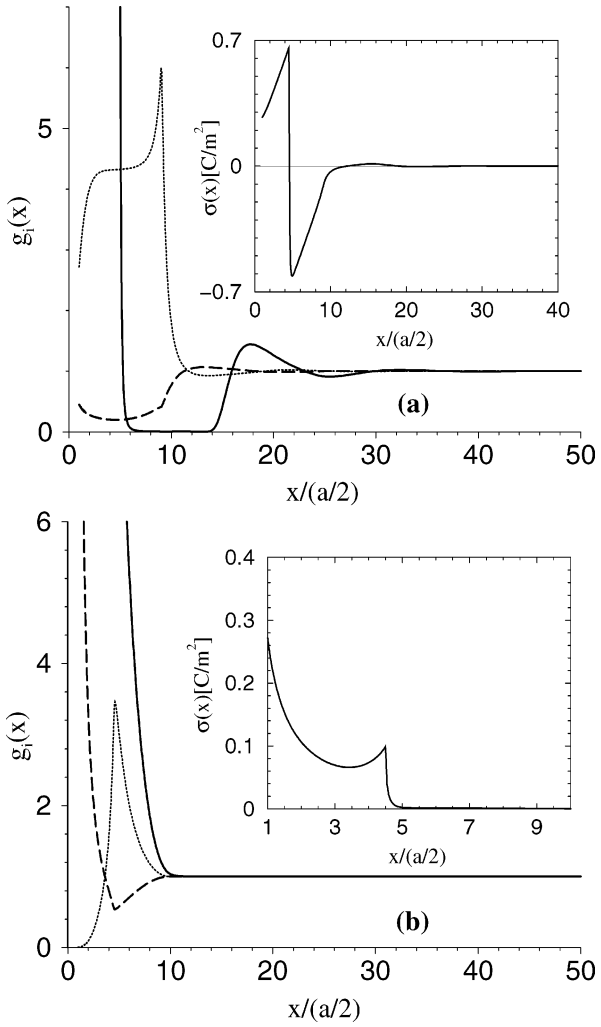

Figure 7. Inhomogeneous RCPs, as a function of x, for macroions (solid line), anions (dashed line), and cations (dotted line) next to a positively charged wall (0.272 C/m^2). The fluid contains macroions ($z_M = -40$, $\rho_M = 0.01$ M, $a_M = 4.5a$) in a 2:1 electrolyte ($\rho_+ = 0.7$ M, $\rho_- = 1.0$ M, $z_+ = 2$, $z_- = -1$). The closest approach distance of the small ions to the wall is $a/2 = 2.125$ Å, and x is measured in units of this quantity. In the inset, the solid line is the charge density profile, $\sigma(x)$, as a function of x. These profiles were obtained from the HNC/MSA theory applied to (a) IEPIM and (b) PIM.

for the IEPIM (Figure 7a) and for the PIM (Figure 7b). As we pointed out above, in the IEPIM, size correlations for the small ions are neglected, whereas in the PIM, size correlations are neglected also for macroions. These results should be contrasted with those of Figure 2, which are for the IPM with the same parameters, where size correlations for all the species are considered. For the IEPIM results, the RCP show that the macroions concentration at the contact with the wall remains nearly the same as for the IPM in Figure 2, i.e., $\rho_M(a_M/2) \approx 21$ M. This indicates that the adsorption of macroions is mainly driven by the strength of the macroion−wall electrostatic attraction and, thus, that the small ions play a minor role in macroion adsorption. The RCP for cations indicate that they surround the macroions in a higher proportion than in the IPM, and the positive ions peak at $\sim 9a/2$ is notably higher than that observed at $\sim 10a/2$ in Figure 2. These differences, in first place, are understood in terms of the macroion−cation Coulombic interaction, i.e., whereas in the IPM, $\xi_{M+} = -24.43$, in the IEPIM, $\xi_{M+} = -29.86$, which explains why point ions are better attracted to surround the macroions than cations with finite size. Additionally, the absence of the steric repulsion (among the little ions in the IEPIM) allows more little ions to gather around the macroions.

More important for our discussion, however, is the decrease of the adsorption of the second macroion layer, $\rho_M(x = 13.5a/2) \approx 0.015$ M, which for the IPM is $\rho_M(x = 15.5a/2) \approx 0.035$ M. Notice that in the IEPIM the second macroion layer is exactly at contact with the first macroion layer, whereas for the IPM, these layers are mediated by a layer of divalent cations. The strong adsorption of cations to the macroions exaggerate very much the OC and CR effects.

In Figure 7b, for the PIM, we observe dramatic changes. First it is now the little negative ions which are strongly adsorbed to the wall, $\rho_-(a/2) \approx 23$ M, instead of the macroions which now have $\rho_M(a_M/2) \approx 3.3$ M, whereas for the IPM and IEPIM $\rho_M(a_M/2) \approx 21$ M. The adsorption of the divalent positive little ions decreases, and they adsorb strongly at the middle of the macroions, i.e., the positive ion RCP is at $\approx 4.5a/2$. The second macroion adsorption layer as well as the OC, CR, and CI completely disappear.

Hence, our results indicate that, when the wall is oppositely charged to the macroions, the first layer of macroions adsorption is energy driven, $U_{\gamma M}$, whereas the second layer is entropy driven, η_T; i.e., the smaller the particles size, the larger the accessible volume, the larger the system entropy, and, hence, the smaller the macroions adsorption. On the other hand, the neglect of the little ion size (IEPIM) implies a higher OC and CR. The neglect of macroion size gives completely unphysical results for the RCPs and charge density profiles, $\sigma_0(x)$.

In Figure 8, we study the IEPIM (Figure 8a) and PIM (Figure 8b) for the case of a negative wall, i.e., the macroions and the wall are now like charged. In parts a and b of Figure 8, the positive little ions are strongly adsorbed to the wall. However this adsorption is about the same as for the IPM, i.e., $\rho_+(a/2) \approx 23$ M for the IEPIM and $\rho_+(a/2) \approx 23$ M for the PIM. In the IEPIM, the macroion adsorption dramatically decreases. This is due to the decrease of the excluded volume, i.e., lower values of η_T. As a consequence, the surface CR decreases in a very important manner.

In Figure 8b, the second layer of the macroion adsorption disappears whereas a first layer appears, $\rho_M(a_M/2) \approx 2.2$ M. The positive little ions strongly adsorb to the macroions, i.e., basically $\eta_T = 0$ and $\xi_{ij} \rightarrow \infty$, $\forall\ i, j = +, -, M$. Hence the first little ion positive layer strongly attracts the macroions, and the absence of short-range correlations allows a large local macroions concentration, which is not higher (in Figure 2, $\rho_M(a_M/2) \approx 21$ M) because $\eta_T = 0$. This anomalous behavior promotes a surface CR at $\sim 4.5a/2$, whereas in Figure 3, this is at $x = 6.5a/2$; i.e., there is one little positive ion between the wall and the macroion layer. On the other hand, while for the IPM there is CI (see Figure 3), for the PIM, there is no CI. Hence, our results indicate that lower η_T implies lower macroion adsorption and lower CR and CI. Although it is not shown, we find that a more (less) negative wall charge density produces greater (lower) macroion adsorption to the wall, mediated by a layer of positive little ions. So, a general conclusion from our result for macroions next to a like-charged wall is that higher wall or macroion charge density or higher macroion size, concentration, and/or high little ion size or concentration increase the macroion adsorption. In other words, for this case also, higher ξ_{ij}, η_T, and $U_{\gamma i}$ increase macroion adsorption, mediated by a layer of little ions, and CR and CI.

In Figure 9, we calculate the IEPIM for the case in which $\sigma_0 = 0$. These results should be compared to Figure 5. The

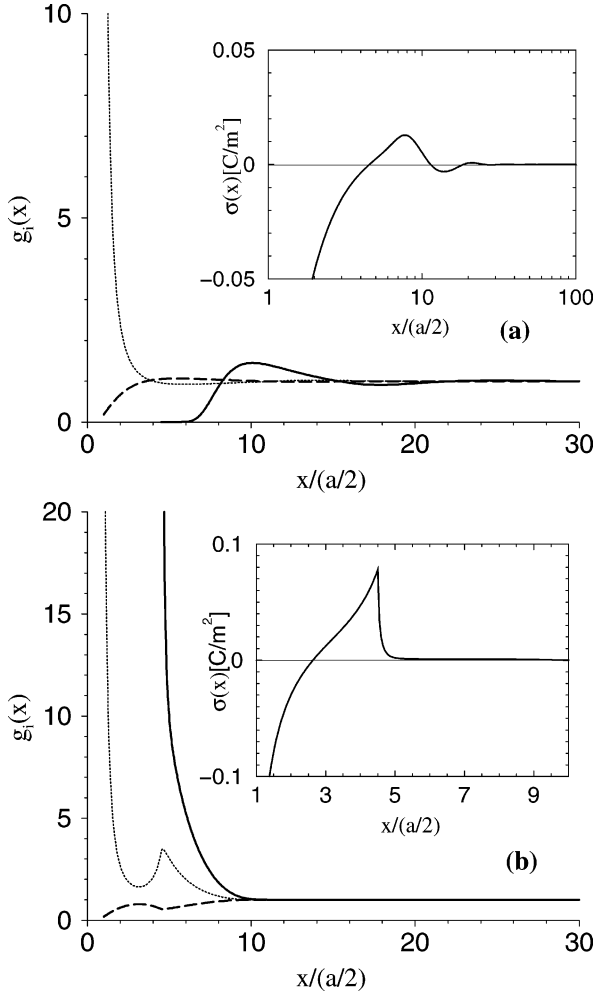

Figure 8. Inhomogeneous RCPs, as a function of x, for macroions, anions, and cations next to a negatively charged wall ($\sigma_0 = -0.272$ C/m^2). The closest approach distance of the point ions to the wall is $a/2 = 2.125$ Å, and x is measured in units of this quantity. In the inset, the solid line is the charge density profile, $\sigma(x)$, as a function of x. The lines and the fluid parameters are as in Figure 7. These profiles were obtained from the HNC/MSA theory applied to (a) IEPIM and (b) PIM.

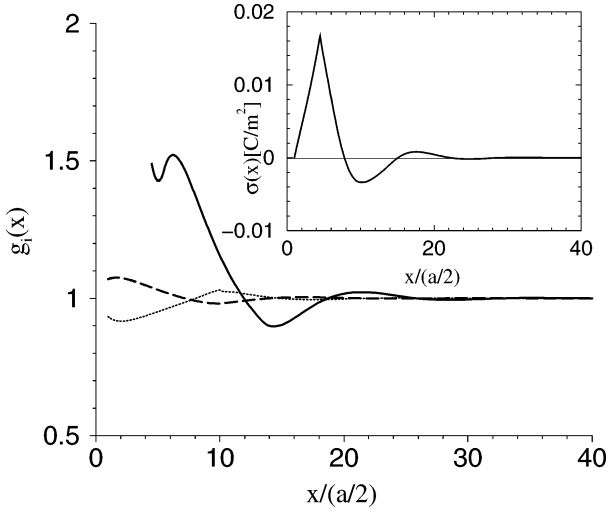

Figure 9. Inhomogeneous RCPs, as a function of x, for macroions, anions, and cations next to an uncharged wall ($\sigma_0 = 0.0$ C/m^2). The closest approach distance of the small ions to the wall is $a/2 = 2.125$ Å, and x is measured in units of this quantity. In the inset, $\sigma(x)$ is plotted. The lines, the fluid, and parameters are as in Figure 5. These profiles were obtained from the HNC/MSA theory applied to the IEPIM.

difference is, of course, the neglect, in Figure 9, of the little ion size. In this simple and important case, we clearly see the short-range correlations effects. The decrease in η_T implies an important lower macroion adsorption, and a qualitative different behavior in the little ions RCPs. While in Figure 5, both positive and negative little ions are strongly adsorbed to the wall, in Figure 9, the positive little ions are significantly less adsorbed to the wall. Clearly the little ion adsorption, in Figure 5, is due to the depletion force, which is absent in the IEPIM, of Figure 9. For both models, the little negative ions are more adsorbed to the wall than the positive ions. Since the macroions are negatively charged, this behavior is apparently unphysical. However, this result can be understood if we remember that the positive ions are divalent, and a simple calculation shows that the total positive *charge* next to the wall is, in fact, larger than the total negative charge. On the other hand, CR and CI in Figure 9 are basically in qualitative agreement with those in Figure 5.

Probably the IEPIM could be a good model for recent experiments where giant like-charged confined macroions in solution are seen to attract each other.[41−44] In the inset, the minimum of $\sigma(x)$ is at $x \approx 10.5a/2$ and is due to the adsorption of macroions (see the main plot). In consequence, a positive charge is induced for $x < a_M/2$ with the maximum at $x = a_M/2$. If no macroions are present ($\rho_M = 0$), $\sigma(x) = 0\ \forall\ x > 0$. Notice the oscillations in the point ion RCP. The classical PB equation is equivalent to consider only a point ion electrolyte; moreover, it is well known that the RCPs obtained from the PB equation next to a charged wall or *around two macroions* (DLVO theory[5,14]) do not show oscillations and that, for the case of the interaction of two macroions at infinite dilution, the macroion−macroion interaction is purely repulsive.[45,46] In fact, it is a mathematical theorem that the PB equation cannot predict an attractive force for two like-charged macroions, between them or with the wall, at infinite dilution.[47] In our study, the adsorption of macroions to the wall implies an *effective* macroion−macroion attraction. The difference between our Figure 9 results, IEPIM, and those of the classical PB is the finite concentration of macroions, which implies a better consideration of entropy. This result could be relevant in the theory of charged fluids and is suggestive in relation to the observed attraction between giant macroions, when they are close to a wall.[41,42] In this respect, notice that, according with the contact value of the macroions concentration profiles, the average distance between two adsorbed macroions is of the order of two macroion diameters. For giant macroions, the distance between two adsorbed like-charged macroions is of the order of micrometers, as observed in some experiments,[41,42] which could be seen as a long-range macroion−macroion attractive interaction.

4. Conclusions

We studied the IPM for macroions in an electrolyte solution by means of a well-established integral equations theory. Our model includes explicitly the electrolyte and macroions with electrostatic and excluded volume interactions. In our study, the Coulomb coupling parameter $\xi_{ij} \equiv \beta/\epsilon\ q_i q_j/a_{ij}$ accounts for the electrostatic correlations, whereas the excluded volume $\eta_T \equiv \pi/6(\rho_+ a_+^3 + \rho_- a_-^3 + \rho_M a_M^3)$ for the steric contribution. Across the paper we have insisted that larger η_T or ξ_{ij} produce a higher particle adsorption and, in consequence, from a compromise between electrostatic and steric effects result in

CR, CI, and OC. We emphasize that OC is defined as the accumulation of an effective charge next to a like-charged wall. This effect results from the adsorption of macroions by an oppositely charged wall, which come accompanied by their counterions, i.e., particles equally charged to the wall. For the occurrence of overcharging, ion−macroion attractive interaction is needed, but more importantly, a high particle excluded volume. *It is found that CR, CI, and OC can occur even for zero wall or macroion charge due to the proper consideration of many-body correlations.* We believe these findings had not been recognized in the past. Our results are consistent with computer simulations for simpler systems[3,4] and some experimental results.[6,41−44] For the simpler two-component asymmetric electrolyte, our results reduce to previous calculations.[8]

In this paper, we studied a three-component macroion solution, we find a more complex manifestation of CR and CI, not reported before, and we find a new effect, OC. We discussed the adsorption mechanisms in terms of the energy and entropy of the system and in terms of three quite general model parameters, ξ_{ij}, η_T, and $U_{\gamma i}$. As a general conclusion, both the hard-core and the electrostatic repulsive interactions produce an attractive force on particles toward the wall. Such a force is conceived as of entropic origin, i.e., the system gains entropy by adsorbing particles to the wall. The electrostatic repulsive interaction between particles confers to them the appearance of a higher excluded volume, and in analogy with the hard spheres fluid, the strength of the attractive depletion force increases by increasing the particle's excluded volume. Therefore, by increasing the effective particle's excluded volume, the adsorption of particles is favored, even if the wall and particles are like charged or uncharged. In other words, by increasing the values of ξ_{ii} and/or η_T, there is a decrease in the system bulk entropy that favors the tendency of particles to be adsorbed.

We point out that, although we have performed calculations for a reduced number of system conditions, the general behavior of the model can be predicted from our results and the use of the parameters $U_{\gamma i}$, ξ_{ij}, and η_T.

From the comparison of the IPM with the IEPIM and PIM, we can conclude that while the IEPIM is in general a qualitative agreement with the IPM, the PIM gives unphysical results. However, we emphasize that the IEPIM has an important quantitative and, in some cases, also qualitative, disagreement, indicating the importance of including short-range correlations in the study of inhomogeneous macroions solutions.

Acknowledgment. We gratefully acknowledge the financial support of INDUSTRIAS NEGROMEX.

Appendix

A. The Mean Spherical Approximation. In our integral equation approach for inhomogeneous fluids, the direct correlation functions, $c_{ij}(s)$, for the particles influenced by the external field is required in eq 12. These functions are approximated by the direct correlation functions for a bulk fluid. In this study, we use the MSA expressions of the $c_{ij}(s)$ functions for a three-component primitive model electrolyte solution obtained by Blum.[48,49] The expression for the direct correlation function can be written as

$$c_{ij}(s) = c_{ij}^{sr}(s) + c_{ij}^{hs}(s) - \beta \frac{z_i z_j e^2}{\epsilon s} \tag{27}$$

with $c_{ij}^{sr}(s) = e^2\beta/\epsilon\ d_{ij}(s)$ and

$$d_{ij}(s) = \begin{cases} \zeta_{ij} + \dfrac{z_i z_j}{s} & \text{for } 0 \le s \le \lambda_{ij} \\ \dfrac{\alpha_{ij} + z_i z_j}{s} - \gamma_{ij} + \eta_{ij} s + \varsigma_{ij} s^3 & \text{for } \lambda_{ij} < s \le a_{ij} \\ 0 & \text{for } s > a_{ij} \end{cases} \tag{28}$$

with $\lambda_{ij} \equiv |a_i - a_j|/2$ and $a_{ij} \equiv (a_i + a_j)/2$. The function $c_{ij}^{hs}(s)$ is the direct correlation function for a hard-spheres binary mixture in the PY approximation. For particles of the same size, it is given by

$$c_{ii}^{hs}(s) = \begin{cases} -\nu_i - \chi_i s - \delta s^3 & \text{if } s < a_i \\ 0 & \text{if } s > a_i \end{cases} \tag{29}$$

For particles of different size, it is given by

$$c_{13}^{hs}(s) = \begin{cases} \alpha_1 & \text{if } s \le \lambda \\ \alpha_1 + \dfrac{\upsilon x^2 + 4\lambda\delta x^3 + \delta x^4}{s} & \text{if } \lambda < s \le a_{13} \\ 0 & \text{if } s > a_{13} \end{cases} \tag{30}$$

with $x = s - \lambda$ and the constants given by

$$s_i = (n_i + \Gamma x_i)$$

$$\zeta_{ij} = 2\left[z_i n_j - x_i s_i + \frac{a_i}{3} s_i^2\right]$$

$$\alpha_{ij} = (a_i - a_j)\left\{\frac{(x_i + x_j)}{4}[s_i - s_j] - \frac{(a_i - a_j)}{16}[(n_i + \Gamma x_i + n_j + \Gamma x_j)^2 - 4n_i n_j]\right\}$$

$$\gamma_{ij} = (x_i - x_j)(n_i - n_j) + (x_i^2 + x_j^2)\Gamma + (a_i + a_j) n_i n_j - \frac{1}{3}[a_i s_i^2 + a_j s_j^2]$$

$$\eta_{ij} = \frac{x_i}{a_i} s_i + \frac{x_j}{a_j} s_j + n_i n_j - \frac{1}{2}[s_i^2 + s_j^2]$$

$$\varsigma_{ij} = \frac{s_j}{6a_j^2} + \frac{s_i}{6a_i^2}$$

where Γ is obtained from the solution of the following algebraic equation

$$\Gamma^2 = \frac{\pi e^2 \beta}{\epsilon} \sum_{i=1}^{n} \rho_i (z_i + n_i a_i)^2 \tag{31}$$

The n_i are obtained from the solution of the following set of algebraic equations

$$-(z_i + n_i a_i)\Gamma = n_i + c a_i \sum_{j=1}^{n} (z_i + n_j a_i) \tag{32}$$

where $c = \pi/2\ [1 - \pi/6 \sum_{j=1}^{n} \rho_i a_i^3]^{-1}$ and the x_i are defined as $x_i \equiv z_i + n_i a_i$

$$\nu_i = \frac{\partial \beta p}{\partial \rho_i}$$

$$\upsilon = -\pi a_{13} g_{13}(a_{13}) \sum_{i=1}^{3} \rho_i a_i g_{ii}(a_i)$$

$$\delta = \frac{\pi}{12} \sum_{i=1}^{3} \rho_i \nu_i$$

$$\chi_1 = \chi_2 = -\pi[\rho_1 a^2 g_{11}{}^2(a) + \rho_2 a^2 g_{22}^2(a) + \rho_3 a_3 g_{13}^2(a_{13})] \tag{33}$$

$$\beta p = \left\{ \rho_T[1 + \eta_T + \eta_T^2] - \frac{\pi}{2} \rho_3(\rho_1 + \rho_2)(a_3 - a)^2 \left[(a + a_3) + a a_3 \frac{\pi}{6} \sum_{i=1}^{3} \rho_i a_i^2 \right] \right\} (1 - \eta_T)^{-3} \tag{34}$$

$$g_{11}(a) = \left\{ \left[1 + \frac{1}{2} \eta_T \right] + \frac{3}{2} \eta_3 a_3^3 (a - a_3) \right\} (1 - \eta_T)^{-2}$$

$$g_{13}(a_{13}) = [a_3 g_{11}(a) + a g_{33}(a_3)]/2a_{13} \tag{35}$$

The expressions for χ_3 and $g_{33}(a_3)$ are obtained by interchanging η_1 and a_1 with η_3 and a_3 in the expressions for χ_1 and $g_{11}(a)$.

The expressions for the functions $K_{ij}(x,y)$ and $L_{ij}(x,y)$ used in eq (12) are given by

$$L_{ji}(x,y) = \int_{|x-y|}^{\infty} c_{ji}^{sr}(s)\, s ds = \frac{e^2 \beta}{\epsilon} D_{ij}(x,y)$$

$$K_{ji}(x,y) = \int_{|x-y|}^{\infty} c_{ji}^{hs}(s)\, s ds \tag{36}$$

By use of eqs 27−30 and taking advantage of cylindrical coordinates, we have

$$K_{ii}(x,y) = \begin{cases} -\nu_i J_2 - \chi_i J_3 - \delta J_5 & \text{for } a_{ii} \geq |x-y| \\ 0 & \text{for } a_{ii} < |x-y| \end{cases} \tag{37}$$

$$K_{13}(x,y) = \begin{cases} \alpha_1 J_2 + \upsilon a^3/3 + \delta \lambda_{13} a^4 + \delta a^5/5 & \text{for } |x-y| < \lambda_{13} \\ \alpha_1 J_2 + \upsilon P_3 + 4\delta \lambda_{13} P_4 + \delta P_5 & \text{for } \lambda_{13} < |x-y| \leq a_{13} \\ 0 & \text{for } a_{13} < |x-y| \end{cases} \tag{38}$$

$$D_{ij}(x,y) = \begin{cases} \zeta_{ij} k_0 + z_i z_j J_1 + \alpha_{ij} M_1 - \gamma_{ij} M_2 + \eta_{ij} M_3 + \varsigma_{ij} M_5 & \text{for } 0 \leq |x-y| \leq \lambda_{ij} \\ (\alpha_{ij} + z_i z_j) J_1 - \gamma_{ij} J_2 + \eta_{ij} J_3 + \varsigma_{ij} J_5 & \text{for } \lambda_{ij} < |x-y| \leq a_{ij} \\ 0 & \text{for } a_{ij} < |x-y| \end{cases} \tag{39}$$

with the following definitions: $J_n = (a_{ij}^n - |x-y|^n)/n$, $P_n = (a^n - (|x-y| - \lambda_{ij})^n)/n$, $M_n = (a_{ij}^n - \lambda_{ij}^n)/n$, and $k_0 = (\lambda_{ij}^2 - (x-y)^2)/2$.

References and Notes

(1) Decher, G. *Science* **1997**, *277*, 1232.
(2) Cuvillier, N.; Rondelez, F. *Thin Solid Films* **1998**, *327−329*, 19.
(3) Tanaka, M.; Grosberg, A. Y. *J. Chem. Phys.* **2001**, *115*, 56.
(4) Terao, T.; Nakayama, T. *Phys. Rev. E* **2002**, *65*, 021405.
(5) Gelbart, W. M.; Bruinsma, R. F.; Pincus, P. A.; Parsegian, V. A. *Phys. Today* **2000**, *59*, 38.
(6) Tohver, V.; Smay, J. E.; Braun, P. V.; Lewis, J. A. *PNAS* **2001**, *98*, 8950.
(7) Attard, P. *J. Phys. Chem.* **1995**, *99*, 14174.
(8) Greberg, H.; Kjellander, R. *J. Chem. Phys.* **1998**, *108*, 2940.
(9) Lozada-Cassou, M.; González-Tovar, E.; Olivares, W. *Phys. Rev. E* **1999**, *60*, R17.
(10) Lozada-Cassou, M.; González-Tovar, E. *J. Colloid Interface Sci.* **2002**, *239*, 285.
(11) Quesada-Pérez, M.; González-Tovar, E.; Martín-Molina, A.; Lozada-Cassou, M.; Hidalgo-Álvares, R. *ChemPhysChem* **2003**, *4*, 234.
(12) Rädler, J. O.; Koltover, I.; Salditt, T.; Safinya, C. R. *Science* **1997**, *275*, 810.
(13) Levin, Y. *Rep. Prog. Phys.* **2002**, *65*, 1577.
(14) Schmitz, K. S. *Macroions in Solution and Colloidal Suspensions*; VCH Publishers: New York, 1993.
(15) Gurovitch, E.; Sens, P. *Phys. Rev. Lett.* **1999**, *82*, 339.
(16) van Megen, W.; Snook, I. *J. Chem. Phys.* **1980**, *73*, 4656.
(17) Gonzáles-Tovar, E.; Lozada-Cassou, M.; Henderson, D. *J. Chem. Phys.* **1985**, *83*, 361.
(18) Mier y Teran, L.; Suh, S. H.; White, H. S.; Davis, H. T. *J. Chem. Phys.* **1990**, *92*, 5087.
(19) Sjöstrom, L.; Åkesson, T.; Jönsson, B. *Ber. Bunsen.−Ges. Phys. Chem.* **1996**, *100*, 889.
(20) Nguyen, T. T.; Grosberg, A. Y.; Shklovskii, B. I. *Phys. Rev. Lett.* **2000**, *85*, 1568.
(21) Totsuji, H. *Phys. Rev. A* **1978**, *17*, 399.
(22) Messina, R.; Holm, C.; Kremer, K. *Phys. Rev. Lett.* **2000**, *85*, 872, which is a *zero*-temperature study.
(23) Muthukumar, M. *J. Chem. Phys.* **1996**, *105*, 5183.
(24) Deserno, M.; Jiménez-Ángeles, F.; Holm, C.; Lozada-Cassou, M. *J. Phys. Chem. B* **2001**, *105*, 10983.
(25) Lozada-Cassou, M.; Saavedra-Barrera, R.; Henderson, D. *J. Chem. Phys.* **1982**, *77*, 5150.
(26) Lozada-Cassou, M.; Olivares, W.; Sulbarán, B. *Phys. Rev. E* **1996**, *53*, 522.
(27) Yu, J.; Degrève, L.; Lozada-Cassou, M. *Phys. Rev. Lett.* **1997**, *79*, 3656
(28) Degrève, L.; Lozada-Cassou, M. *Phys. Rev. E* **1998**, *57*, 2978.
(29) Jiménez-Ángeles, F.; Lozada-Cassou, M. *J. Phys. Chem. B* **2004**, *108*, 1719.
(30) Lozada-Cassou, M. *J. Chem. Phys.* **1981**, *75*, 1412.
(31) Lozada-Cassou, M. In *Fundamentals of inhomogeneous fliuds*; Henderson, D., Ed.; Marcel Dekker: New York, 1993; Chapter 8.
(32) McQuarrie, D. A. *Statistical Mechanics*; Harper Collins Publishers, Inc.: New York, 1976.
(33) Friedman, H. L. *A Course in Statistical Mechanics*; Prentice Hall: Englewood Cliffs, NJ, 1985.
(34) Lozada-Cassou, M. *J. Chem. Phys.* **1984**, *80*, 3344.
(35) Lozada-Cassou, M.; Díaz-Herrera, E. *J. Chem. Phys.* **1990**, *93*, 1386.
(36) We remind that the total volume, V, is the space where particles are contained, whereas the excluded volume, υ, is defined as the *effective* fraction of V, occupied by the particles. Finally, the accessible volume, $\upsilon' = V - \upsilon$, is the free unoccupied volume, within V, left by the particles.
(37) Trokhymchuk, A.; Henderson, D.; Nikolov, A.; Wassan, D. T. *Phys. Rev. E* **2001**, *64*, 012401.
(38) Kaplan, P. D.; Rouke, J. L.; Youdh, A. G.; Pine, D. J. *Phys. Rev. Lett.* **1994**, *72*, 582.
(39) Mier y Terán, L.; Díaz-Herrera, E.; Lozada-Cassou, M.; Saavedra-Barrera, R. *J. Comput. Phys.* **1989**, *84*, 326.
(40) Terao, T.; Nakayama, T. *Phys. Rev. E* **2001**, *63*, 041401.
(41) Kepler, G. M.; Fraden, S. *Phys. Rev. Lett.* **1994**, *73*, 356.
(42) Crocker, J. C.; Grier, D. G. *Phys. Rev. Lett.* **1996**, *77*, 1897.
(43) Grier, D. G. *Nature* **1998**, *393*, 621.
(44) Han, Y.; Grier, D. G. *Phys. Rev. Lett.* **2003**, *91*, 038302.
(45) Attard, P. *Adv. Chem. Phys.* **1996**, *92*, 1.
(46) Sánchez, J. E.; Lozada-Cassou, M. *Chem. Phys. Lett.* **1992**, *190*, 202.
(47) Neu, J. C. *Phys. Rev. Lett.* **1999**, *82*, 1072.
(48) Blum, L. *Mol. Phys.* **1975**, *30*, 1529.
(49) Kazuo, H. *Mol. Phys.* **1977**, *33*, 1195.